ACS APPLIED MATERIALS & INTERFACES

Research Article

www.acsami.org

Yolk–Shell Nanoarchitectures with a Ru-Containing Core and a Radially Oriented Mesoporous Silica Shell: Facile Synthesis and Application for One-Pot Biomass Conversion by Combining with Enzyme

Wei Wei, Yu Zhao, Shichao Peng, Haoyang Zhang, Yipeng Bian, Hexing Li, and Hui Li*

Education Ministry Key Lab of Resource Chemistry and Shanghai Key Laboratory of Rare Earth Functional Materials, Shanghai Normal University, Shanghai 200234, P. R. China

Supporting Information

ABSTRACT: In this paper, we develop a facile strategy for fabricating a yolk–shell structured catalytic system that consists of a core made of Ru supported on mesoporous carbon, which is encaged within a silica shell that has ordered radial mesochannels. A region-selective etching mechanism for the formation of the yolk–shell nanoarchitectures is proposed based on the stronger adsorption ability of the carbon core for etching agent than that of the silica shell for etching agent. By combining such material with amyloglucosidase, one-pot hydrolysis–hydrogenation of dextrin to sorbitol can be conducted, delivering enhanced efficiency and showing great promise for biomass conversion applications.

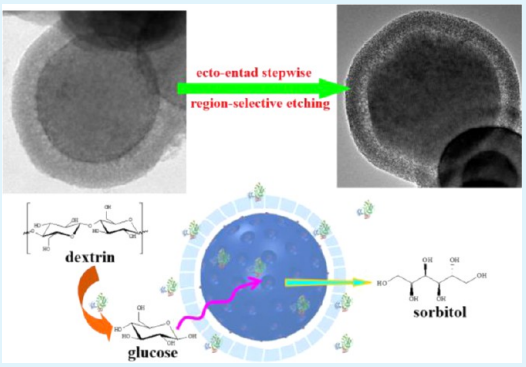

KEYWORDS: *yolk–shell nanostructure, mesoporous material, metallic catalysis, enzymatic catalysis, biomass conversion, sorbitol*

INTRODUCTION

Controllable integration of diverse materials into well-defined yolk–shell micro/nanoarchitectures has attracted immense attention in many important research fields, such as drug delivery, energy storage, as well as catalysis.[1−11] In the domain of catalysis, encaging a functional material within a porous material with a certain thickness to generate a yolk–shell configuration not only brings unique collective and synergetic function in comparison with the single-component materials,[6] but also protects the individual core.[12] Recently, for instance, Liu et al. successfully developed a general method to generate yolk–shell structures using a vesicle templating approach,[13] which can encapsulate metallic nanoparticles[14] or enzyme[15] within the void space and provide protective function. Generally, such special yolk–shell structures are routinely fabricated by layer-by-layer coating the sacrificial template and the shell material on the surface of a functional core, followed by a subsequent intermediate layer removal.[10] Presently, several selective etching strategies for synthesizing yolk–shell architectures from core–shell multilayer materials have been reported, including acid etching,[6,16] alkali etching,[1,3,17] organo-silicone-assisted etching,[18] and hot-water etching.[2] However, these processes are quite complex since multistep deposition of materials and selective removal of the sacrificial template are generally necessary for achieving the yolk–shell structures. From the viewpoint of practical applications, exploring more simple approaches to preparing yolk–shell architectures is an important issue.

Sorbitol, a valuable platform molecule that can be facilely transformed into fuels or chemicals,[19] is usually produced via hydrogenation of glucose,[20−26] obtained mostly by enzymatic hydrolysis of starches.[27−29] Obviously, one-pot hydrolysis–hydrogenation of starch to sorbitol displays advantages in simplifying operation process and lowering the cost mainly linked to separation and refining procedures.[30−32] Amorphous alloys, metastable materials with long-range disordered but short-range ordered structure, have attracted growing attention from both academia and industry because of their superior catalytic properties to their crystalline counterparts.[33] Ru–B amorphous alloy has proved to be a potential alternative to metallic Ru and Raney Ni in hydrogenation of glucose to sorbitol.[34] However, our recent studies[35] revealed that the amyloglucosidase is easily poisoned when contacting with Ru-based catalysts. Meanwhile, the metallic Ru active sites would be covered by the amyloglucosidase and the colloidal substances originated from dextrin hydrolysis, leading to a rapid deactivation for the subsequent glucose hydrogenation to sorbitol. To tackle these problems, we had designed a yolk–shell structured catalytic system that consists of a highly

Received: August 8, 2014
Accepted: November 18, 2014
Published: November 18, 2014

Scheme 1. Illustration of the Synthesis Process of Yolk−Shell Structured Ru−B/mCarbon@air@mSiO$_2$

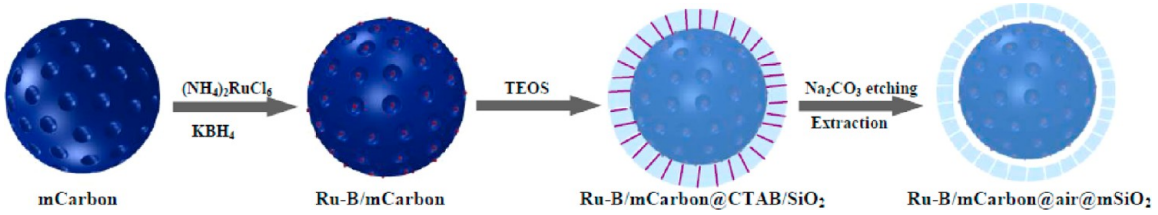

dispersed Ru−B amorphous alloy on the ordered mesoporous silica encaged within a porous silica shell (Ru−B/mSiO$_2$@air@SiO$_2$).[35] One-pot hydrolysis−hydrogenation of dextrin can be successfully conducted to produce sorbitol by the combination of amyloglucosidase with the yolk−shell structured Ru−B/mSiO$_2$@air@SiO$_2$, where the silica shell separated the incompatible catalysts in different regions. More specifically, the enzymatic dextrin hydrolysis to glucose occurred in the bulk solution outside Ru−B/mSiO$_2$@air@SiO$_2$ owing to the blocking effect of the silica shell. Meanwhile, the permeation-selective silica shell allowed the diffusion of the small glucose molecules into the catalytically active core (Ru−B/mSiO$_2$) for hydrogenation to sorbitol. Nevertheless, several drawbacks are present in this system. First, the preparation of Ru−B/mSiO$_2$@air@SiO$_2$ involved multistep deposition of materials to generate sandwich-structured precursor and a subsequent selective removal of the middle layer, complicating the synthetic process. Second, the production of sorbitol from dextrin included harsh reaction conditions (348 K and hydrogen pressures up to 6 MPa), which increased the operation risk and decreased the economic attractiveness. Finally, the silica shell was formed as disordered mesoporous material, which is unfavorable for catalytic activity because of the presence of mass transport.

Herein, we report the design of a yolk−shell structured material that consists of a catalytically active Ru core (Ru supported on mesoporous carbon, Ru−B/mCarbon) and a silica shell that has radially oriented ordered mesochannels (mSiO$_2$). The combination of such material (Ru−B/mCarbon@air@mSiO$_2$) with amyloglucosidase enables efficient one-pot hydrolysis−hydrogenation of dextrin to sorbitol under mild conditions. The design concept used in such yolk−shell structured catalyst can be extended to other compositions for cascade reactions containing incompatible parameters.

EXPERIMENTAL PROCEDURES

Material Preparation. Phenol, formaldehyde, sodium hydroxide (NaOH), F127 ($PEO_{106}PPO_{70}PEO_{106}$), $(NH_4)_2RuCl_6$, potassium borohydride (KBH_4), cetyltrimethylammonium bromide (CTAB), tetraethoxysilane (TEOS), dodecanol, ethanol, sodium carbonate (Na_2CO_3), $NH_3{\cdot}H_2O$, hydrofluoric acid (HF), dextrin, and amyloglucosidase (glucoamylase; *exo*-1,4-α-glucosidase; EC 3.2.1.3 from *Aspergillus niger*; 100 000 units/ml) were purchased from Aladdin Industrial Co., Ltd. (Shanghai, China) and were used without any other treatments.

The synthesis of yolk−shell Ru−B/mCarbon@air@mSiO$_2$ is in three steps (Scheme 1).

(1) Uniform dispersion of Ru−B amorphous alloys within the porous channels of ordered mesoporous carbon nanospheres (Ru−B/mCarbon) was achieved by ultrasound-assisted incipient wetness infiltration of $(NH_4)_2RuCl_6$ onto mCarbon, followed by the reduction with borohydride.[36] First, mCarbon was synthesized following the method described by Zhao's group.[37] Briefly, 1.6 g of phenol was dissolved in 30 mL of 0.1 M NaOH aqueous solution, followed by adding 5.6 mL of formaldehyde aqueous solution (37 wt %). The mixture was stirred at 343 K for 0.5 h, followed by adding 30 mL of F127 aqueous solution containing 1.33 g of F127. After being stirred at 339 K for 2 h with a low stirring speed, 100 mL of H_2O was added. During the reaction, the color of the aqueous solution turned from colorless transparent to pink and finally turned to crimson. After 17 h, the reaction was stopped when the precipitate was observed. Then, 17.7 mL of the obtained solution was transferred into an autoclave and diluted with 56 mL of H_2O, heated at 403 K for 24 h. The solid product was thoroughly washed with deionized water and dried at room temperature. The carbonization and removal of the applied triblock copolymer templates were carried out at 973 K in N_2 atmosphere for 3 h, and the final product mCarbon was obtained. Next, the supported Ru−B catalyst was prepared as follows:[36] 0.6 g of mCarbon was impregnated with a certain mount of $(NH_4)_2RuCl_6$ aqueous solution (0.02 g/50 mL), which was sonicated for 15 min. After impregnation of 12 h, the products were dried at 373 K for 0.5 h. Then, 6 mL of KBH_4 aqueous solution (0.027 g/mL) was added dropwise at 273 K. After being stirred continuously until no bubbles were released, the solid was washed free from Cl^- and K^+ ions with deionized water until a pH of ∼7 was achieved.

(2) The Ru−B/mCarbon was coated by condensation of TEOS in the presence of CTAB, generating a core−shell structured Ru−B/mCarbon@CTAB/SiO$_2$, where CTAB/SiO$_2$ refers to a mesostructured CTAB/silica composite coated on the surface of the Ru−B/mCarbon core. The core−shell structured Ru−B/mCarbon@CTAB/SiO$_2$ was fabricated according to a modified surfactant-templating approach reported by Deng et al.[38] Typically, 0.6 g of Ru−B/mCarbon was dispersed in a mixed solution comprised of 0.4 g of CTAB, 0.12 g of NaOH, 148 μL of dodecanol, 108 mL of ethanol, and 200 mL of water. The mixed solution was sonicated for 15 min and stirred for 1 h at 333 K. Then, 6.4 mL of TEOS was added dropwise into the previous mixture and stirred for 3 h at 333 K. After being thoroughly washed with ethanol and deionized water, the core−shell structured Ru−B/mCarbon@CTAB/SiO$_2$ was obtained.

(3) The as-synthesized core−shell structured Ru−B/mCarbon@CTAB/SiO$_2$ was region-selectively etched with a certain amount of Na_2CO_3 aqueous solution to achieve a yolk−shell structured configuration. In a typical run of synthesis, 1.5 g of Ru−B/mCarbon@CTAB/SiO$_2$ was added to 400 mL of 1.0 M Na_2CO_3 aqueous solution and stirred for 1 h. Afterward, the product was refluxed in acetone for 48 h at 333 K to remove the pore-generating template. This procedure was repeated twice to ensure complete removal of CTAB. Finally, the template-removed yolk−shell structured Ru−B/mCarbon@air@mSiO$_2$ was obtained by centrifugation and washing with plenty of water.

Material Characterization. The bulk composition and Ru loading were analyzed by means of inductively coupled plasma optical emission spectrometry (ICP-OES; Varian VISTA-MPX). The amorphous structure was investigated by both X-ray diffraction (XRD; Rigaku D/Max-RB with Cu Kα radiation) and selective-area electronic diffraction (SAED; JEOL JEM2100). The material shapes and morphologies were observed by both field emission scanning electron microscopy (FESEM; HITACHI S-4800) and transmission

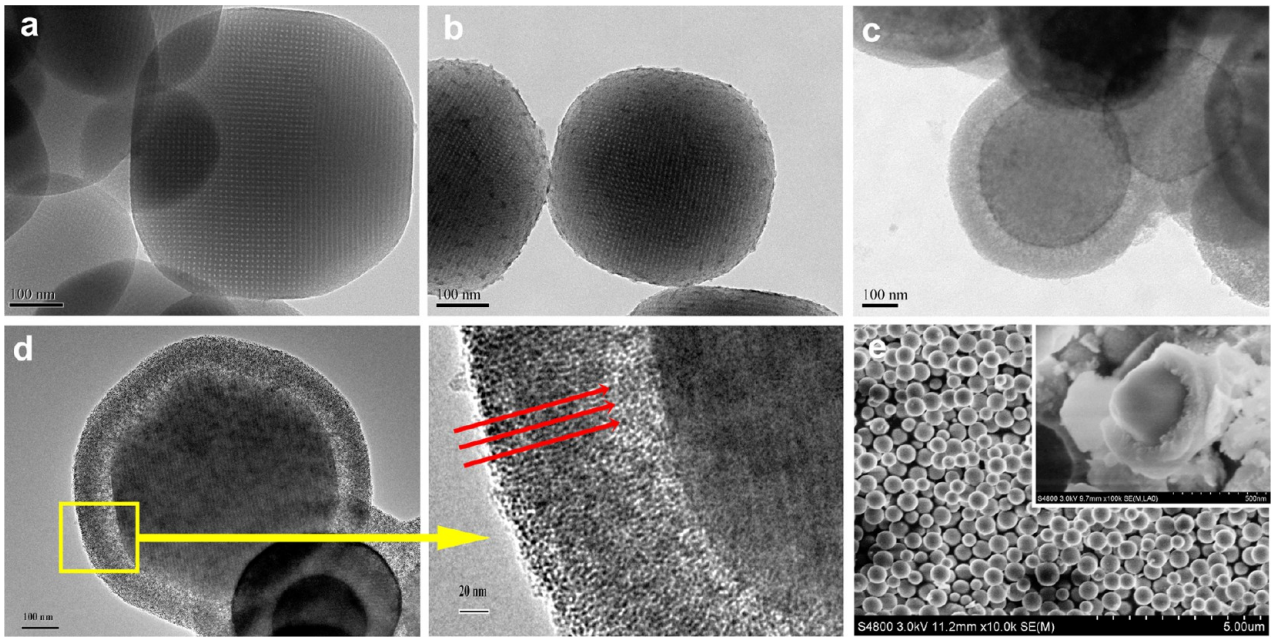

Figure 1. TEM images of (a) mCarbon, (b) Ru−B/mCarbon, (c) Ru−B/mCarbon@CTAB/SiO_2, and (d) Ru−B/mCarbon@air@mSiO_2. (e) FESEM image of Ru−B/mCarbon@air@mSiO_2. (inset) A partially crushed sphere.

electron microscopy (TEM, JEOL JEM2100). The presence of the Ru-containing core and the silica shell was determined by high-angle annular dark-field scanning transmission electron microscopy (HAADF-STEM; FEI Tecnai G2 F20 S-TWIN) and the energy dispersive X-ray spectroscopy (EDS) line scan. N_2 adsorption−desorption isotherms were obtained at 77 K using a Micromeritics TriStar II apparatus. By N_2 adsorption, the Brunauer−Emmett−Teller (BET) surface area (S_{BET}) was calculated by using the multiple-point BET method in the relative pressure range of P/P_0 = 0.05−0.2. The pore volume and pore size distribution curve were obtained by the Barrett−Joyner−Halenda model. The surface electronic states were determined by X-ray photoelectron spectroscopy (XPS; ULVAC-PHI PHI5000 VersaProbe system using Al Kα radiation), during which all samples were pretreated in situ in a pure Ar atmosphere to avoid oxidation.

Activity Test. In a typical experiment, the one-pot hydrolysis−hydrogenation of dextrin to sorbitol was carried out in a Parr 4848 autoclave containing yolk−shell structured Ru−B/mCarbon@air@mSiO_2 (15.6 mg Ru), 0.048 mL of amyloglucosidase, 0.6 g of dextrin, 60 mL of water, and 4.0 MPa of H_2 at 343 K. The reaction system was stirred vigorously (800 rpm) to eliminate the diffusion effect. The reaction mixture was sampled at intervals for product analysis on a liquid-phase chromatograph (Agilent 1200) equipped with a carbohydrate column (Shodex, SC1011) and a refractive index detector at 333 K with water as the movable phase at 0.6 mL/min. After the mixture cooled to room temperature at the end of the reaction, the yolk−shell structured catalyst was separated by centrifugation and washed with ethanol and deionized water for further characterization and applications. To test the catalyst durability, the used Ru−B/mCarbon@air@mSiO_2 catalyst was centrifuged and washed thoroughly with ethanol and deionized water after each run of the reaction. Then, the Ru−B/mCarbon@air@mSiO_2 was reused with a fresh charge of dextrin and fresh amyloglucosidase for subsequent recycle run under the same reaction conditions.

RESULTS AND DISCUSSION

Structural Characteristics. TEM images (Figure 1a and Supporting Information, Figure S1a) of the as-synthesized mCarbon display uniform spheres with average diameters of ∼550 nm and consists of ordered mesoporous channels. The pore size is roughly estimated to be ∼3 nm. The N_2 adsorption−desorption isotherm, pore size distribution curve, and low-angle XRD pattern of the as-synthesized mCarbon (Supporting Information, Figure S2) further confirm the ordered mesostructure centered approximate 3 nm with high S_{BET} of 489 m^2 g^{-1}. Figure 1b and Supporting Information, Figure S1b demonstrate that Ru−B/mCarbon with Ru loading of 2.21 wt % and atom composition of $Ru_{71}B_{29}$ contains similar mesostructure to the parent mCarbon and that the Ru−B NPs are uniformly dispersed into the pore channels. From Figure 1c and Supporting Information, Figure S1c, one can see that the Ru−B/mCarbon core is completely coated by silica shell with a thickness of ∼100 nm without significant damage to either the ordered mesoporous channels of mCarbon or the uniform distribution of Ru−B NPs. Figure 1d and Supporting Information, Figure S1d reveal that, after being etched with Na_2CO_3 aqueous solution, the thickness of silica shell decreased by ∼10 nm, together with the formation of a space ∼10 nm between the silica shell and the Ru−B/mCarbon core. From the high-magnification TEM image of the yolk−shell structured particles in Figure 1d, both the smooth outer surface and the rough inner surface can be clearly observed for the silica shell, obviously due to the selective removal of the partial inner shell section. Again, no significant damage to either the ordered mesoporous structure of mCarbon or the uniform distribution of Ru−B NPs was observed in the Ru−B/mCarbon@air@mSiO_2. Moreover, it is significant to note that the mesochannels in the outer silica shell are continuous throughout the shell with openings at surface and radially oriented to the sphere surface. Such a unique pore orientation is due to the perpendicular alignment of surfactant mesophases induced by the equal attractivity to polar and nonpolar species of the interface between the CTAB/silica phase and the water/ethanol solution.[39−41] The perpendicular mesoporosity in the silica shell is anticipated to increase the accessibility of the Ru−B/mCarbon core and enhance the efficiency of mass transport. The pore size in the silica shell can be roughly measured to be 4 nm. FESEM image (Figure 1e) reveals that the yolk−shell

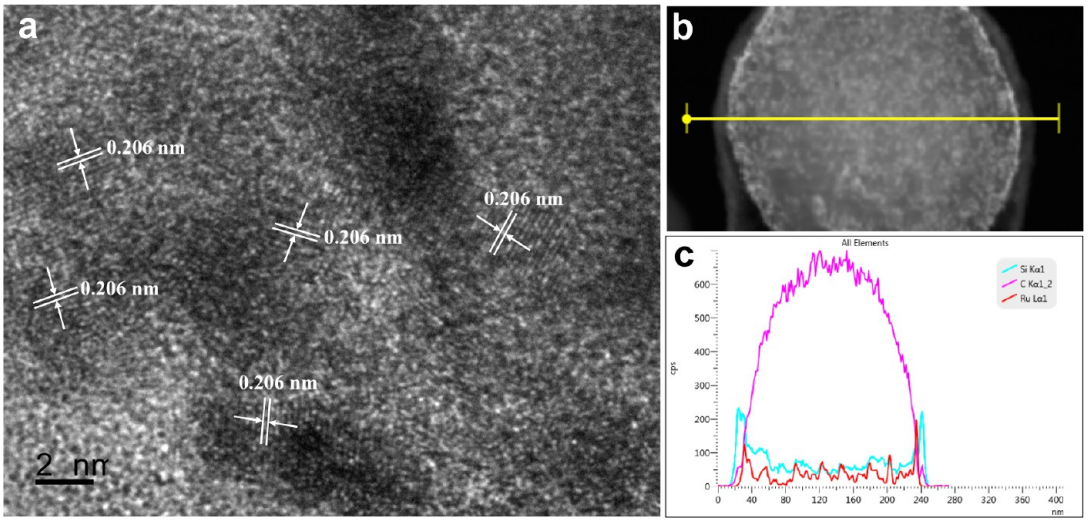

Figure 2. (a) HRTEM image, (b) HAADF-STEM image, and (c) EDS line scanning profiles of Ru−B/mCarbon@air@$mSiO_2$.

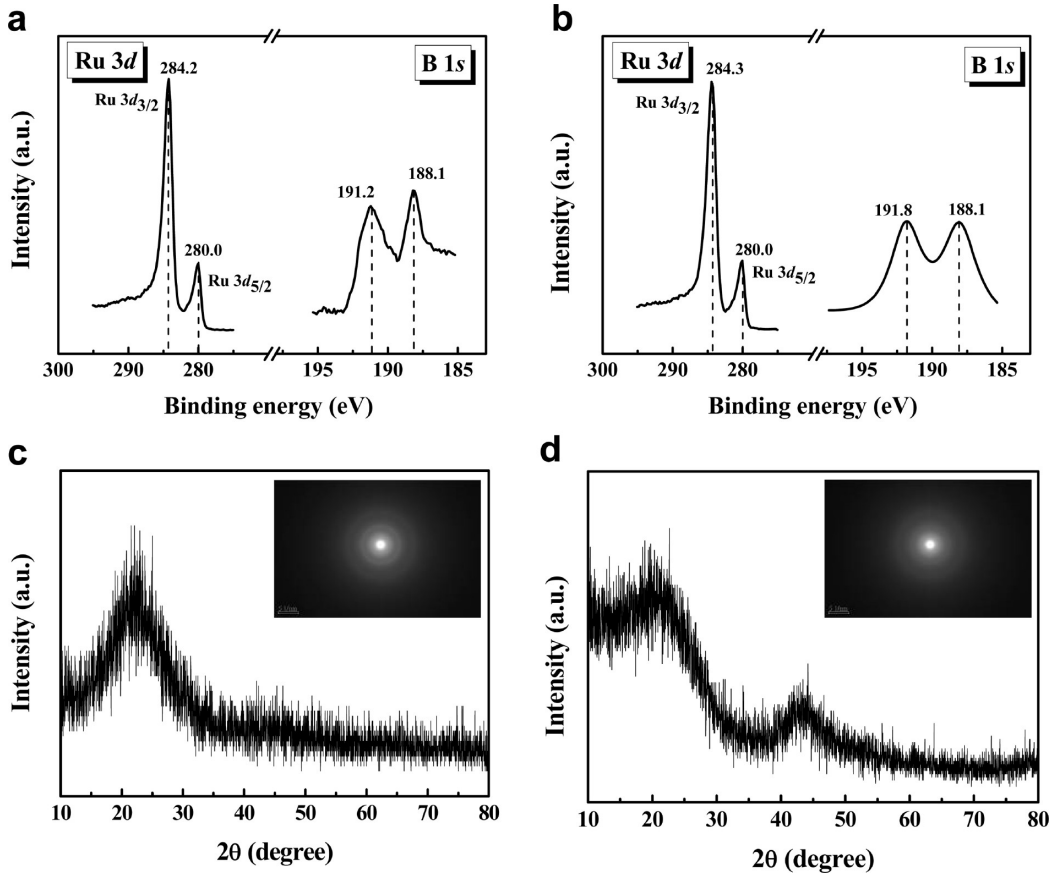

Figure 3. XPS spectra of (a) Ru−B/mCarbon and (b) Ru−B/mCarbon@air@$mSiO_2$. Wide-angle XRD patterns of (c) Ru−B/mCarbon and (d) Ru−B/mCarbon@air@$mSiO_2$. (insets) SAED images of the Ru−B particles.

structured Ru−B/mCarbon@air@$mSiO_2$ displays uniformly spheres, which is in good agreement with the TEM results. The attached FESEM image of broken Ru−B/mCarbon@air@$mSiO_2$ further confirms the yolk−shell structure (inset in Figure 1e). The high-resolution TEM (HRTEM) characterization of Ru−B/mCarbon@air@$mSiO_2$ was carried out (Figure 2a), which exhibited several Ru nanoparticles with crystalline lattices. All the *d*-spacings were ca. 0.206 nm, which matched with {101} of Ru (hcp, PDF 06−0663) well. To further confirm the presence of the Ru-containing core and the silica shell, an image was obtained by HAADF-STEM for Ru−B/mCarbon@air@$mSiO_2$, which was recorded in STEM Dark Field (DF) mode (Figure 2b). The STEM-DF mode could enhance the contrast of heavy metal atoms by collecting the high-angle incoherent scattering signals, which clearly demonstrated the locations and distribution of Ru nanoparticles in the core. Meanwhile, the EDS line scanning for different elements including Si, C, and Ru across Ru−B/mCarbon@air@$mSiO_2$

dx.doi.org/10.1021/am5052608 | *ACS Appl. Mater. Interfaces* 2014, 6, 20851−20859

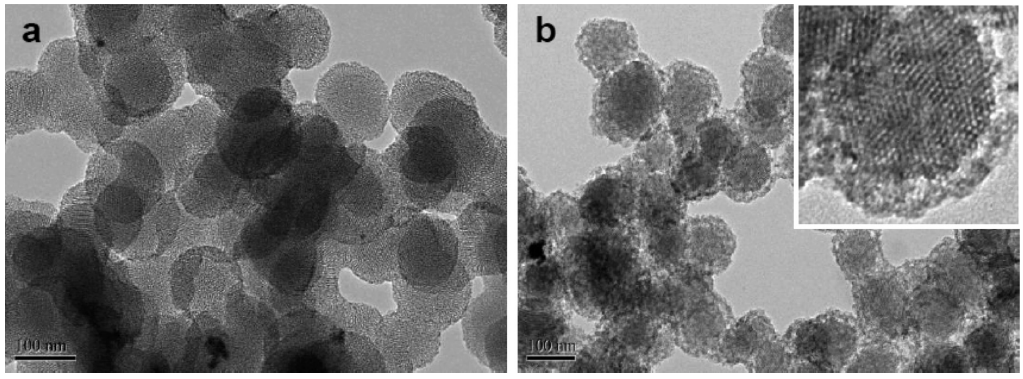

Figure 4. TEM images of (a) $mSiO_2$@CTAB/SiO_2 and (b) $mSiO_2$@air@$mSiO_2$.

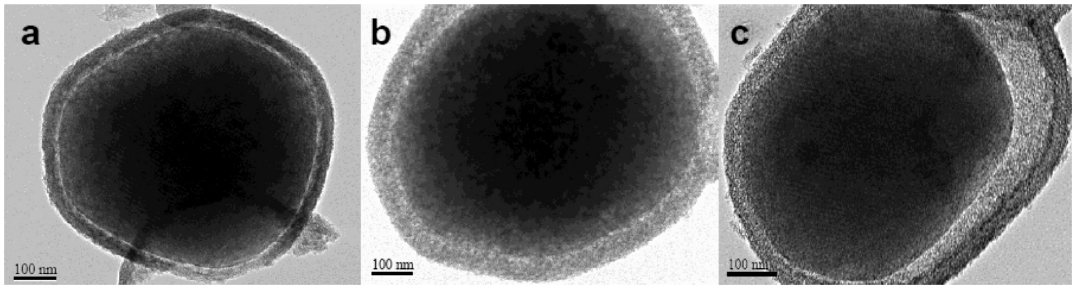

Figure 5. TEM images of the Ru−B/mCarbon@air@$mSiO_2$ synthesized with different etchants (etching conditions): (a) NaOH aqueous solution (7.2 mL, 0.10 g/mL, 3 h), (b) concentrated ammonia aqueous solution (800 mL, 27 wt %, 2 h), and (c) HF aqueous solution (80 mL, 0.3 wt %, 40 min).

(Figure 2c) confirmed the locations of Ru in the mCarbon core and the presence of silica shell.

The XPS spectra (Figure 3a,b) demonstrate that all the Ru species in both the Ru−B/mCarbon and the yolk−shell structured Ru−B/mCarbon@air@$mSiO_2$ are present in metallic state, corresponding to the binding energy (BE) of 280.0 eV in Ru $3d_{5/2}$; while the B species are present in elemental state and B_2O_3 with BE of 188.1 and 191.2 eV in B 1s level. The BE of the elemental B is shifted positively by 1.0 eV in comparison with the BE of pure B,[42] suggesting the formation of Ru−B alloy in which partial electrons transfer from B to Ru. No significant BE shift of metallic Ru is observed, possibly due to its relatively big atomic size compared to the B atom. The wide-angle XRD patterns (Figure 3c,d) reveal that the Ru−B alloys in both the Ru−B/mCarbon and the Ru−B/mCarbon@air@$mSiO_2$ are present in a typical amorphous alloy structure state, corresponding to a broad peak at $\sim 2\theta = 45°$,[43] which is further confirmed by the consecutive diffraction halos in the attached SAED pictures.[44] As a result, the XPS and XRD data, coupled with that of SAED, confirmed the formation of Ru−B amorphous alloy.

Formation Process. Some control experiments were implemented to verify this region-selective etching strategy further. It is well-known that carbon has stronger adsorption ability compared with silica materials.[45,46] Accordingly, the Ru−B/mCarbon is anticipated to facilitate the enrichment of the etching agent to induce the ecto-entad stepwise removal of the inner shell section. In contrast with the observation that the yolk−shell structured Ru−B/mCarbon@air@$mSiO_2$ still retains the smooth outer surface of the $mSiO_2$ shell (Figure 1d), the result of an experiment using MCM−41-type mesoporous silica nanospheres ($mSiO_2$) instead of mCarbon (other conditions keep constant) revealed that the inner and the outer surfaces of the shell were damaged simultaneously since both surfaces were rather rough (Figure 4). Furthermore, significant damage to the surface of the $mSiO_2$ core can be clearly observed in $mSiO_2$@air@$mSiO_2$. These are mainly due to the equal adsorption ability of the core and the shell in $mSiO_2$@air@$mSiO_2$ for etchant, which can lead to the simultaneous etching of the inner and the outer shell section, even the surface of the core. Except for the stronger adsorption ability of mCarbon core for the etching agent relative to the $mSiO_2$ shell, the inertness of carbon to etching agent might be another factor responsible for the formation of yolk−shell structure via region-selective etching mechanism. Another control experiment (Supporting Information, Figure S3) revealed that mCarbon is inert to Na_2CO_3 aqueous solution, which allows the removal of the inner shell of silica rather than the carbon core.

During the synthesis of Ru−B/mCarbon@air@$mSiO_2$, prolonging the etching time from 1 to 2 h resulted in the increase of the void between the Ru−B/mCarbon core and the $mSiO_2$ shell (Supporting Information, Figure S4), even the appearance of Ru−B/mCarbon particles without $mSiO_2$ shell (marked with arrow in Supporting Information, Figure S4), further demonstrating the ecto-entad stepwise etching process.

Besides the etching time, both the concentration of Na_2CO_3 aqueous solution and the etching temperature are also important for obtaining well-defined yolk−shell structured Ru−B/mCarbon@air@$mSiO_2$. As confirmed by TEM images (Supporting Information, Figure S5), etching the shell with low concentration of etchant (0.5 M) or at low temperature (273 K) could not achieve evident cavity between the core and the shell. However, an etchant solution with much higher concentration (2.0 M) or much more elevated etching

Scheme 2. One-Pot Hydrolysis–Hydrogenation of Dextrin to Sorbitol by Combination of Enzymatic with Metallic Catalysis

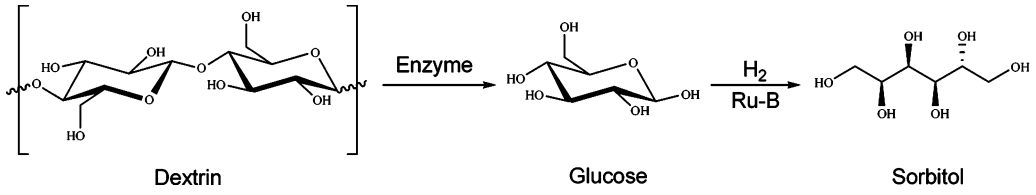

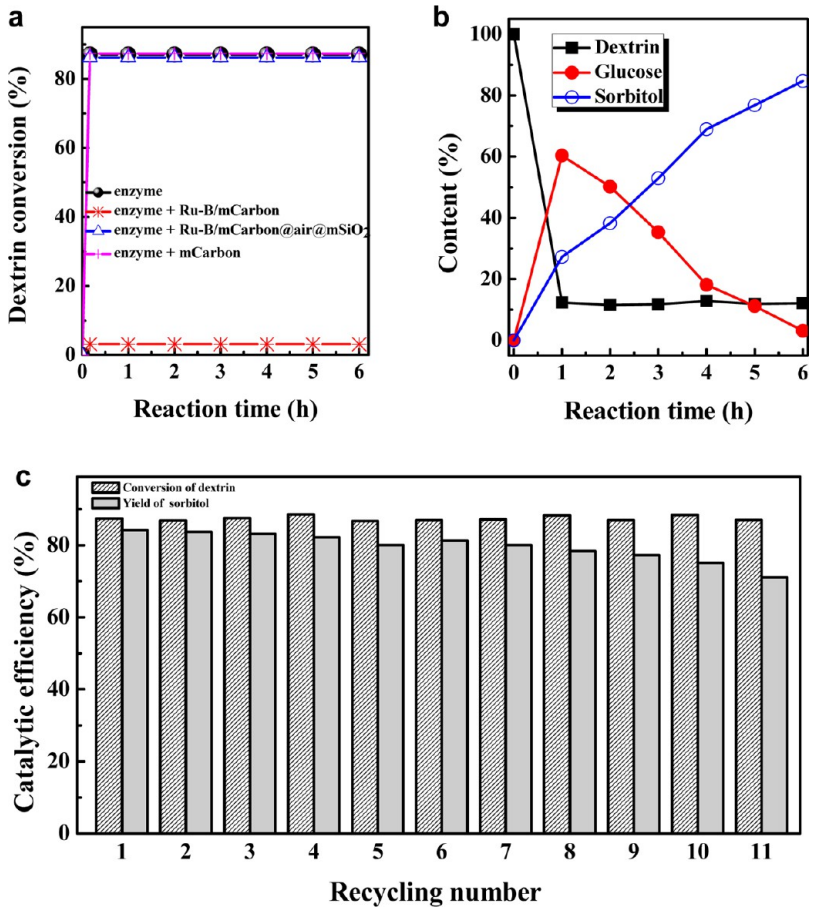

Figure 6. (a) Dextrin hydrolysis in different catalyst systems. (b) Reaction profile and (c) recycling test of the combination of amyloglucosidase and Ru–B/mCarbon@air@$mSiO_2$ for one-pot hydrolysis–hydrogenation of dextrin. Reaction conditions: dextrin (0.6 g), amyloglucosidase (0.048 mL), a catalyst (containing 15.6 mg of Ru), water (60 mL), T = 343 K, P_{H2} = 4.0 MPa, stirring rate = 800 rpm. Each run was conducted for 6 h in recycling test.

temperature (323 K) could completely dissolve the $mSiO_2$ shell and produce unencapsulated Ru–B/mCarbon particles.

More interestingly, the yolk–shell structured Ru–B/mCarbon@air@$mSiO_2$ can be achieved from the core–shell structured Ru–B/mCarbon@CTAB/SiO_2 by using diverse etchants, such as NaOH, ammonia, and HF aqueous solution, under respectively optimal conditions (Figure 5), demonstrating the generality of this region-selective etching strategy.

Catalytic Performances. One-pot conversion of dextrin to sorbitol (Scheme 2) was used as a test reaction to evaluate the performances of the catalyst system including free amyloglucosidase and the yolk–shell structured Ru–B/mCarbon@air@$mSiO_2$. Figure 6a shows the enzymatic efficiency of amyloglucosidase for dextrin hydrolysis in different catalyst systems. Note that dextrin hydrolysis was carried out using amyloglucosidase accompanying mCarbon or Ru–B/mCarbon, and negligible and significant inhibiting effects on the activity can be observed, respectively. This implies that amyloglucosidase is easily poisoned once directly contacting with metallic Ru, in line with results reported in our recent studies.[35] Hardly any change in the dextrin hydrolysis efficiency of amyloglucosidase can be detected in the presence of the yolk–shell structured Ru–B/mCarbon@air@$mSiO_2$, obviously thanks to the protective effect of the $mSiO_2$ shell that prevents amyloglucosidase from entering the chamber to contact the Ru–B/mCarbon core. Because the amyloglucosidase (100–1000 nm), the dextrin molecule, and other colloidal substances resulting from the dextrin hydrolysis (more than 1000 nm)[35] are far bigger than the pore size in the $mSiO_2$ shell (4 nm), they cannot diffuse through the $mSiO_2$ shell, efficiently avoiding the poisoning effects. Taking into account that the molecular size of glucose is relatively small (~1 nm), the $mSiO_2$ shell allows the liberated glucose via dextrin hydrolysis to diffuse into the Ru–B/mCarbon core, followed by hydrogenation to sorbitol over the Ru–B amorphous alloys (Figure 6b). For comparison, we also removed the CTAB templates from Ru–B/mCarbon@

CTAB/SiO_2 to obtain the core−shell structured Ru−B/mCarbon@$mSiO_2$. As shown in Supporting Information, Figure S6, the sorbitol yields in the catalyst system containing amyloglucosidase and Ru−B/mCarbon@$mSiO_2$ are much lower than those catalyzed by amyloglucosidase and the yolk−shell structured Ru−B/mCarbon@air@$mSiO_2$ throughout the whole reaction process. This further confirms the key role played by the cavity between the Ru−B/mCarbon core and the $mSiO_2$, which not only increases the accessibility of glucose molecules to the catalytically active core metals, but also promotes the glucose hydrogenation efficiency owing to the enrichment of reactants and the enhancement of the collision frequency between reactants and Ru active sites in the chamber,[47−51] as reported in our recent publication.[35] Compared with our previous work (348 K, 6 MPa of H_2),[35] the present design of Ru−B/mCarbon@air@$mSiO_2$ enables the one-pot production of sorbitol from dextrin to proceed under milder reaction conditions (343 K, 4 MPa of H_2). Meanwhile, only a shorter reaction time (6 h) in the present catalyst system is needed to achieve a sorbitol yield similar to that of the previous report (7 h). Taking into account that the dextrin hydrolysis efficiencies of amyloglucosidase can be retained in both the catalyst systems, the enhanced catalytic efficiency of the present system should be due to the superior glucose hydrogenation activity of the Ru−B/mCarbon@air@$mSiO_2$ to the Ru−B/$mSiO_2$@air@SiO_2 (Figure 7). On one hand, the higher electrical conductivity and adsorption capability of mCarbon over $mSiO_2$[52] favor the glucose hydrogenation over Ru active sites. On the other hand, the presence of radical mesochannels further contributes to the glucose transferring,[14,53] as confirmed by the activity comparison between Ru−B/mCarbon@air@$mSiO_2$ and Ru−B/mCarbon@air@SiO_2, Ru−B/mCarbon encaged within disordered silica (Figure 7).

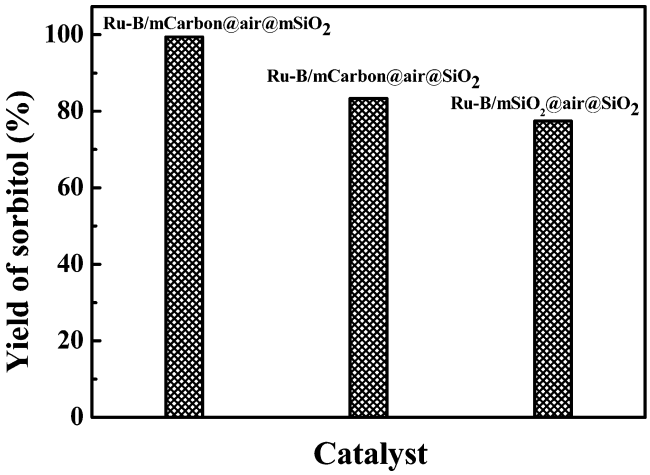

Figure 7. Comparison of glucose hydrogenation efficiencies over different yolk−shell structured catalysts. Reaction conditions: glucose (0.6 g), a catalyst (containing 15.6 mg of Ru), water (60 mL), T = 343 K, P_{H2} = 4.0 MPa, stirring rate = 800 rpm.

Besides the high efficiency, the Ru−B/mCarbon@air@$mSiO_2$ could be easily separated from the reaction solution via centrifugation and used repetitively for more than 11 times with only 13% decrease of sorbitol yield in one-pot dextrin conversion (Figure 6c). During the recycling test, the used yolk−shell structured catalyst had no influence on the efficiency of amyloglucosidase for dextrin hydrolysis (Figure 6c). Therefore, the slight decrease of sorbitol yield after the 11th cycle should be due to the partial loss of activity for glucose hydrogenation. ICP-OES analysis and XRD experiment (Supporting Information, Figure S7) could rule out the leaching of Ru active sites and the crystallization of the amorphous alloy structure of Ru−B in Ru−B/mCarbon@air@$mSiO_2$ after being reused for 11 times. The TEM images (Figure 8) showed that Ru−B/mCarbon@air@$mSiO_2$ was still present in yolk−shell structure morphology after 11th cycle. However, partial collapse of the pore of mCarbon can be observed after being used repetitively for 11 times, which might be the main factor responsible for the decrease in activity. Immobilization of amylogulosidase directly onto the outer surface of $mSiO_2$ shell is needed in future work to ensure that a real merging of such yolk−shell nanostructures and enzyme can be achieved.

CONCLUSIONS

In summary, we developed a simple approach for synthesizing a yolk−shell structured catalytic system that consists of a Ru−B/mCarbon core and a silica shell with ordered radial mesochannels (Ru−B/mCarbon@air@$mSiO_2$). On the basis of the stronger adsorption ability for etching agent of mCarbon than that of $mSiO_2$, a region-selective etching mechanism to form such yolk−shell structure is proposed. In particular, our present method is more facile and cost-effective since no additional steps are needed to coat a layer of sacrificial template and remove it. Thus, this strategy can potentially be extended to other yolk−shell structures with different composition, size, and shape. The one-pot production of sorbitol from dextrin study highlights the role of the mesoporous silica shell in the Ru−B/mCarbon@air@$mSiO_2$, which enables the sequential reaction containing incompatible parameters to take place in

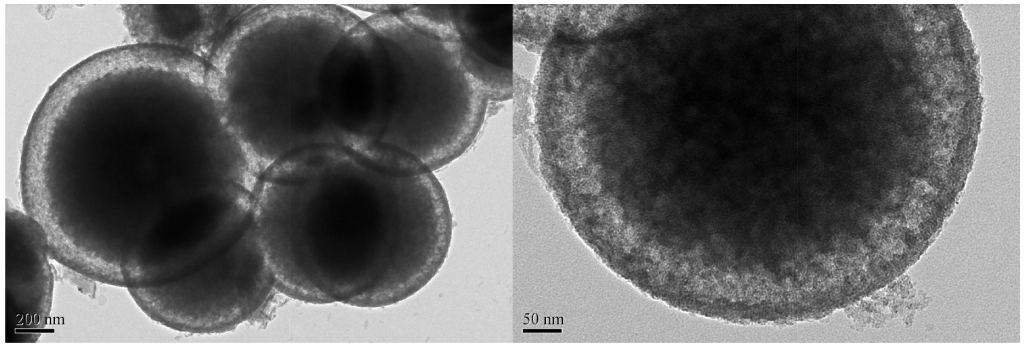

Figure 8. TEM images of the Ru−B/mCarbon@air@$mSiO_2$ catalyst after being reused for 11 times.

one pot. This might provide a preferable method for the one-pot cascade reactions.

■ ASSOCIATED CONTENT

Supporting Information

Low-magnification TEM images of mCarbon, Ru−B/mCarbon, Ru−B/mCarbon@CTAB/SiO_2, and Ru−B/mCarbon@air@$mSiO_2$; adsorption/desorption isotherm, the corresponding pore size distribution curve, and low-angle XRD pattern of the as-synthesized mCarbon; TEM images of pure mCarbon and $mSiO_2$ and the samples after being etched in Na_2CO_3 aqueous solution; TEM image of the sample synthesized by similar conditions to those used to synthesize Ru−B/mCarbon@air@$mSiO_2$ but prolonging the etching time to 2 h; TEM images of the samples synthesized by similar conditions to those used to synthesize Ru−B/mCarbon@air@$mSiO_2$ but with low concentration (0.5 M) or high concentration (2.0 M) of Na_2CO_3 aqueous solution and at low etching temperature (273 K) or high etching temperature (323 K); dependency of sorbitol yield on the reaction time in one-pot hydrolysis−hydrogenation of dextrin by combining amyloglucosidase and Ru−B/mCarbon@$mSiO_2$ or Ru−B/mCarbon@air@$mSiO_2$; wide-angle XRD pattern of the Ru−B/mCarbon@air@$mSiO_2$ after being reused for 11 times. This material is available free of charge via the Internet at http://pubs.acs.org.

■ AUTHOR INFORMATION

Corresponding Author

*Phone: +86-21-64323578. Fax: +86-21-64322272. E-mail: lihui@shnu.edu.cn.

Notes

The authors declare no competing financial interest.

■ ACKNOWLEDGMENTS

This work was supported by the National Natural Science Foundation of China (21273149), PCSIRT (IRT1269), the Program for New Century Excellent Talents in University (NCET-11-1052), and the Shanghai Science & Technology and Education Committee (11JC1408900, 12490502800, 10SG41, 12YZ084).

■ REFERENCES

(1) Zhang, F.; Braun, G. B.; Shi, Y. F.; Zhang, Y. C.; Sun, X. H.; Reich, N. O.; Zhao, D. Y.; Stucky, G. Fabrication of Ag@SiO_2@Y_2O_3 Nanostructures for Bioimaging: Tuning of the Upconversion Fluorescence with Silver Nanoparticles. *J. Am. Chem. Soc.* **2010**, *132*, 2850−2851.

(2) Wong, Y. J.; Zhu, L. F.; Teo, W. S.; Tan, Y. W.; Yang, Y. H.; Wang, C.; Chen, H. Y. Revisiting the Stober Method: Inhomogeneity in Silica Shells. *J. Am. Chem. Soc.* **2011**, *133*, 11422−11425.

(3) Li, W.; Deng, Y. H.; Wu, Z. X.; Qian, X. F.; Yang, J. P.; Wang, Y.; Gu, D.; Zhang, F.; Tu, B.; Zhao, D. Y. Hydrothermal Etching Assisted Crystallization: A Facile Route to Functional Yolk-Shell Titanate Microspheres with Ultrathin Nanosheets-Assembled Double Shells. *J. Am. Chem. Soc.* **2011**, *133*, 15830−15833.

(4) Liu, J.; Qiao, S. Z.; Chen, J. S.; Lou, X. W.; Xing, X. R.; Lu, G. Q. Yolk/shell Nanoparticles: New Platforms for Nanoreactors, Drug Delivery and Lithium-Ion Batteries. *Chem. Commun.* **2011**, *47*, 12578−12591.

(5) Park, J. C.; Song, H. Metal@Silica Yolk−Shell Nanostructures as Versatile Bifunctional Nanocatalysts. *Nano Res.* **2011**, *4*, 33−49.

(6) Yang, Y.; Liu, X.; Li, X. B.; Zhao, J.; Bai, S. Y.; Liu, J.; Yang, Q. H. A Yolk−Shell Nanoreactor with a Basic Core and an Acidic Shell for Cascade Reactions. *Angew. Chem., Int. Ed.* **2012**, *51*, 9164−9168.

(7) Zhang, Q.; Lee, I.; Joo, J. B.; Zaera, F.; Yin, Y. D. Core−Shell Nanostructured Catalysts. *Acc. Chem. Res.* **2013**, *46*, 1816−1824.

(8) Pérez-Lorenzo, M.; Vaz, B.; Salgueiriño, V.; Correa-Duarte, M. A. Hollow-Shelled Nanoreactors Endowed with High Catalytic Activity. *Chem.—Eur. J.* **2013**, *19*, 12196−12211.

(9) Teng, Z. G.; Wang, S. J.; Su, X. D.; Chen, G. T.; Liu, Y.; Luo, Z. M.; Luo, W.; Tang, Y. X.; Ju, H. X.; Zhao, D. Y.; Lu, G. M. Facile Synthesis of Yolk−Shell Structured Inorganic Organic Hybrid Spheres with Ordered Radial Mesochannels. *Adv. Mater.* **2014**, *26*, 3741−3747.

(10) Chen, Y.; Chen, H. R.; Shi, J. L. Construction of Homogenous/Heterogeneous Hollow Mesoporous Silica Nanostructures by Silica-Etching Chemistry: Principles, Synthesis, and Applications. *Acc. Chem. Res.* **2014**, *47*, 125−137.

(11) Li, G. D.; Tang, Z. Y. Noble Metal Nanoparticle@Metal Oxide Core/Yolk-Shell Nanostructures as Catalysts: Recent Progress and Perspective. *Nanoscale* **2014**, *6*, 3995−4011.

(12) Ren, N.; Yang, Y. H.; Shen, J.; Zhang, Y. H.; Xu, H. L.; Gao, Z.; Tang, Y. Novel, Efficient Hollow Zeolitically Microcapsulized Noble Metal Catalysts. *J. Catal.* **2007**, *251*, 182−188.

(13) Liu, J.; Qiao, S. Z.; Hartono, S. B.; Lu, G. Q. Monodisperse Yolk-Shell Nanoparticles with a Hierarchical Porous Structure for Delivery Vehicles and Nanoreactors. *Angew. Chem., Int. Ed.* **2010**, *49*, 4981−4985.

(14) Liu, J.; Yang, H. Q.; Kleitz, F.; Chen, Z. G.; Yang, T. Y.; Strounia, E.; Lu, G. Q.; Qiao, S. Z. Yolk-Shell Hybrid Materials with a Periodic Mesoporous Organosilica Shell: Ideal Nanoreactors for Selective Alcohol Oxidation. *Adv. Funct. Mater.* **2012**, *22*, 591−599.

(15) Zhao, Z. Y.; Liu, J.; Hahn, M.; Qiao, S. Z.; Middelberg, A. P. J.; He, L. Z. Encapsulation of Lipase in Mesoporous Silica Yolk-Shell Sphers with Enhanced Enzyme Stability. *RSC Adv.* **2013**, *3*, 22008−22013.

(16) Chen, D.; Li, L. L.; Tang, F. Q.; Qi, S. Facile and Scalable Synthesis of Tailored Silica "Nanorattle" Structures. *Adv. Mater.* **2009**, *21*, 3804−3807.

(17) Roca, M.; Haes, A. J. Silica@Void@Gold Nanoparticles: Temporally Stable Surface-Enhanced Raman Scattering Substrates. *J. Am. Chem. Soc.* **2008**, *130*, 14273−14279.

(18) Yang, Y.; Liu, J.; Li, X. B.; Liu, X.; Yang, Q. H. Organosilane-Assisted Transformation from Core−Shell to Yolk−Shell Nanocomposites. *Chem. Mater.* **2011**, *23*, 3676−3684.

(19) Corma, A.; Iborra, S.; Velty, A. Chemical Routes for the Transformation of Biomass into Chemicals. *Chem. Rev.* **2007**, *107*, 2411−2502.

(20) Fedor, W. S.; Millar, J.; Accola, A. J. Sorbitol. *Ind. Eng. Chem.* **1960**, *52*, 282−286.

(21) Kruse, W. M.; Wright, L. W. Homogeneous Catalytic Hydrogenation of Sugars. *Carbohydr. Res.* **1978**, *64*, 293−296.

(22) Gallezot, P.; Cerino, P. J.; Blanc, B.; Fleche, G.; Fuertes, P. Glucose Hydrogenation on Promoted Raney-Nickel Catalysts. *J. Catal.* **1994**, *146*, 93−102.

(23) Li, H.; Li, H. X.; Deng, J. F. Glucose Hydrogenation over Ni−B/SiO_2 Amorphous Alloy Catalyst and the Promoting Effect of Metal Dopants. *Catal. Today* **2002**, *74*, 53−63.

(24) Kusserow, B.; Schimpf, S.; Claus, P. Hydrogenation of Glucose to Sorbitol over Nickel and Ruthenium Catalysts. *Adv. Synth. Catal.* **2003**, *345*, 289−299.

(25) Schimpf, S.; Louis, C.; Claus, P. Ni/SiO_2 Catalysts Prepared with Ethylenediamine Nickel Precursors: Influence of the Pretreatment on the Catalytic Properties in Glucose Hydrogenation. *Appl. Catal., A* **2007**, *318*, 45−53.

(26) Sapunov, V. N.; Grigoryev, M.; Ye; Sulman, E.; Konyaeva, M. M. B.; Matveeva, V. G. D-Glucose Hydrogenation over Ru Nanoparticles Embedded in Mesoporous Hypercrosslinked Polystyrene. *J. Phys. Chem. A* **2013**, *117*, 4073−4083.

(27) Yankov, D.; Dobreva, E.; Beschkov, V.; Emanuilova, E. Study of Optimum Conditions and Kinetics of Starch Hydrolysis by Means of Thermostable α-amylase. *Enzyme Microb. Technol.* **1986**, *8*, 665−667.

(28) Hoover, R. Acid-Treated Starches. *Food Rev. Int.* **2000**, *16*, 369−39.

(29) Kadokawa, J. Precision Polysaccharide Synthesis Catalyzed by Enzymes. *Chem. Rev.* **2011**, *111*, 4308−4345.
(30) Bruggink, A.; Schoevaart, R.; Kieboom, T. Concepts of Nature in Organic Synthesis: Cascade Catalysis and Multistep Conversions in Concert. *Org. Process Res. Dev.* **2003**, *7*, 622−640.
(31) Simons, C.; Hanefeld, U.; Arends, I. W. C. E.; Maschmeyer, T.; Scheldon, R. A. Towards Catalytic Cascade Reactions: Asymmetric synthesis Using Combined Chemo-Enzymatic Catalysts. *Top. Catal.* **2006**, *40*, 35−44.
(32) Climent, M. J.; Corma, A.; Iborra, S. Heterogeneous Catalysts for the One-Pot Synthesis of Chemicals and Fine Chemicals. *Chem. Rev.* **2011**, *111*, 1072−1133.
(33) Chen, Y. Chemical Preparation and Characterization of Metal-Metalloid Ultrafine Amorphous Alloy Particles. *Catal. Today* **1998**, *44*, 3−16.
(34) Guo, H. B.; Li, H. X.; Zhu, J.; Ye, W. H.; Qiao, M. H.; Dai, W. L. Liquid Phase Glucose Hydrogenation to D-glucitol over an Ultrafine Ru-B Amorphous Alloy Catalyst. *J. Mol. Catal. A* **2003**, *200*, 213−221.
(35) Xu, L.; Wei, W.; Li, H. X.; Li, H. Combination of Enzyme and Ru−B Amorphous Alloy Encapsulated in Yolk-Shell Silica for One-Pot Dextrin Conversion to Sorbitol. *ACS Catal.* **2014**, *4*, 251−258.
(36) Wang, Y.; Xu, L.; Xu, L.; Li, H. X.; Li, H. Synthesis of Ru-B Amorphous Alloy Supported on SBA-15 with Excellent Catalytic Efficiency in Maltose Hydrogenation. *Chin. J. Catal.* **2013**, *34*, 1027−1032.
(37) Fang, Y.; Gu, D.; Zou, Y.; Wu, Z. X.; Li, F. Y.; Che, R. C.; Deng, Y. H.; Tu, B.; Zhao, D. Y. Low-Concentration Hydrothermal Synthesis of Biocompatible Ordered Mesoporous Carbon Nanospheres with Tunable and Uniform Size. *Angew. Chem., Int. Ed.* **2010**, *49*, 7987−7991.
(38) Deng, Y. H.; Qi, D. W.; Deng, C. H.; Zhang, X. M.; Zhao, D. Y. Superparamagnetic High-Magnetization Microspheres with an Fe_3O_4@SiO_2 Core and Perpendicularly Aligned Mesoporous SiO_2 Shell for Removal of Microcystins. *J. Am. Chem. Soc.* **2008**, *130*, 28−29.
(39) Tan, B.; Rankin, S. E. Interfacial Alignment Mechanism of Forming Spherical Silica with Radially Oriented Nanopores. *J. Phys. Chem. B* **2004**, *108*, 20122−20129.
(40) Yoon, S. B.; Kim, J. Y.; Kim, J. H.; Park, Y. J.; Yoon, K. R.; Park, S. K.; Yu, J. S. Synthesis of Monodisperse Spherical Silica Particles with Solid Core and Mesoporous Shell: Mesopore Channels Perpendicular to the Surface. *J. Mater. Chem.* **2007**, *17*, 1758−1761.
(41) Deng, Y. H.; Cai, Y.; Sun, Z. K.; Liu, J.; Liu, C.; Wei, J.; Li, W.; Liu, C.; Wang, Y.; Zhao, D. Y. Multifunctional Mesoporous Composite Microspheres with Well-Designed Nanostructure: A Highly Integrated Catalyst System. *J. Am. Chem. Soc.* **2010**, *132*, 8466−8473.
(42) Li, H.; Li, H. X.; Dai, W. L.; Wang, W. J.; Fang, Z. G.; Deng, J. F. XPS Studies on Surface Electronic Characteristics of Ni−B and Ni−P Amorphous Alloy and Its Correlation to Their Catalytic Properties. *Appl. Surf. Sci.* **1999**, *152*, 25−34.
(43) Pei, Y.; Zhou, G. B.; Luan, N.; Zong, B. N.; Qiao, M. H.; Tao, F. Synthesis and Catalysis of Chemically Reduced Metal−metalloid Amorphous Alloys. *Chem. Soc. Rev.* **2012**, *41*, 81409−8162.
(44) Klein, S.; Martens, J. A.; Parton, R.; Vercruysse, K.; Jacobs, P. A.; Maier, W. F. Amorphous Microporous Mixed Oxides as Selective Redox Catalyst. *Catal. Lett.* **1996**, *38*, 209−214.
(45) Vanderborght, B. M.; Van Grieken, R. E. Enrichment of Trace Metals in Water by Adsorption on Activated Carbon. *Anal. Chem.* **1977**, *49*, 311−316.
(46) Wang, H.; Qin, H. Q.; Xiong, Z. C.; Zhang, W. B.; Zou, H. F. Facile Synthesis of Yolk-shell Magnetic Mesoporous Carbon Microspheres for Efficient Enrichment of Low Abundance Peptides. *Nanoscale* **2013**, *5*, 10936−10944.
(47) Santiso, E. E.; George, A. M.; Heath Turner, C.; Kostov, M. K.; Gubbins, K. E.; Buongiorno-Nardelli, M.; Sliwinska-Bartkowias, M. Adsorption and Catalysis: The Effect of Confinement on Chemical Reactions. *Appl. Surf. Sci.* **2005**, *252*, 766−777.
(48) Pan, X. L.; Fan, Z. L.; Chen, W.; Ding, Y. J.; Luo, H. Y.; Bao, X. H. Enhanced Ethanol Production Inside Carbon-Nanotube Reactors Containing Catalytic Particles. *Nat. Mater.* **2007**, *6*, 507−511.
(49) Zhu, Y.; Liu, F. P.; Ding, W. P.; Guo, X. F.; Chen, Y. Noncrystalline Metal−Boron Nanotubes: Synthesis, Characterization, and Catalytic-Hydrogenation Properties. *Angew. Chem., Int. Ed.* **2006**, *45*, 7211−7214.
(50) Pan, X. L.; Bao, X. H. Reactions over Catalysts Confined in Carbon Nanotubes. *Chem. Commun.* **2008**, 6271−6281.
(51) Mo, M.; Han, L.; Lv, J. G.; Zhu, Y.; Peng, L. M.; Guo, X. F.; Ding, W. P. Noncrystalline NiPB Nanotubes for Hydrogenation of P-chloronitrobenzene. *Chem. Commun.* **2010**, *46*, 2268−2270.
(52) Dai, H. Carbon Nanotubes: Synthesis, Integration, and Properties. *Acc. Chem. Res.* **2002**, *35*, 1035−1044.
(53) Yang, J. P.; Shen, D. K.; Zhou, L.; Li, W.; Zhao, D. Y. Spatially Confined Fabrication of Core−Shell Gold Nanocages@Mesoporous Silica for Near-Infrared Controlled Photothermal Drug Release. *Chem. Mater.* **2013**, *25*, 3030−3037.